Electronic Supplementary Material (ESI) for Physical Chemistry Chemical Physics.

Supporting Information to

Theoretical description of alkali metal *closo*-boranes – towards the crystal structure of $MgB_{12}H_{12}$

Aristea E. Maniadaki and Zbigniew Łodziana

Institute of Nuclear Physics PAN, ul. Radzikowskiego 152, 31-342 Kraków, Poland.

Calculation methods

The Brilouin zone sampling was performed at k-point grid with density $2 \times 2 \times 2$ for the low temperature $Li_2B_{12}H_{12}$ and $3 \times 2 \times 3$ for the low temperature $Na_2B_{12}H_{12}$. Atoms are represented by the projector augmented method (PAW) [1,2] pseudopotentials with valence electronic configurations $2s^1$ for Li, $2s^2 2p^1$ for B, $3s^1$ for Na, $3s^2$ for Mg, and $1s^1$ for H. Exchange correlation functional was approximated by the Local Density Approximation(LDA) [3] and the General Gradient Approximation (GGA-PBE) [4] parametrization. The ground state electronic density was determined by iterative diagonalization of the Kohn-Sham Hamiltonian with Gaussian smearing 0.05 eV . The relaxation of the atomic structures was performed with the conjugate gradient method with the residual force convergence criteria 10^{-3} eV/Å. For the optimization of the unit cell successive relaxation of the internal atomic positions and the lattice parameters were preformed. For $Li_2B_{12}H_{12}$ and $Na_2B_{12}H_{12}$, the wave functions are expanded in the plane wave basis set with the kinetic energy cutoff 500 eV. For the $MgB_{12}H_{12}$ the kinetic energy cutoff was 700 eV. Convergence tests are presented below.

The charge density analysis was performed as Bader charge analysis implemented by Henkelman *et al.* [5] as well as noncovalent interactions index (NCI) method [6,7], through the Critic2 software [8,9].

Thermodynamic analysis

The calculations of the phonon density of states (pDOS) were performed with the Phonopy package [10]. The force constant matrix was calculated with the finite displacement method (amplitude of displacement ± 0.02 Å). For accuracy assessment the comparison with linear response method [11] was performed. For the phonon calculation additional dense grid was used for the charge density in order to improve accuracy of calculated forces.

For the thermodynamic stability assessments the additional calculations were performed for the reference structures of metal hydrides (LiH, NaH, MgH_2), metal borohydrides ($Mg(BH_4)_2$), and pure elements (Li, Na, Mg, B, H_2). Increased accuracy was used for calculations of the elastic properties of $MgB_{12}H_{12}$.

For the calculation of Gibbs free energy($G_{reaction}$) at temperature T of reaction, the following equations are used:

$$\Delta G_{reaction} = \Delta H - T \cdot \Delta S \tag{1}$$

with the difference in the enthalpy(ΔH) defined as

$$\Delta H = \sum_p (E_p^{TOT} + F_p^{vib}) - \sum_r (E_r^{TOT} + F_r^{vib}) \tag{2}$$

where E^{TOT} is the electronic total energy , F^{vib} the enthalpy of each compound (eq. 4) and p and r denote products and reactants respectively. The entropy difference (ΔS) is defined as

$$\Delta S = S_p^{vib} - S_r^{vib} \tag{3}$$

In the harmonic approximations the enthalpy of a solid, at temperature T is: [12,13]

$$F^{vib}(T) = E_{ZPE} + k_B T \cdot \sum e_i \cdot (e^{-\beta e_i} - 1)^{-1} \tag{4}$$

and the entropy:

$$S^{vib} = \sum [-k_B \cdot ln(1 - e^{-\beta e_i}) + \frac{e_i}{T \cdot (e^{\beta e_i} - 1)} \tag{5}$$

with the zero point energy defined as $E_{ZPE} = \frac{1}{2} \cdot \sum e_i$ and $\beta = 1/(k_B T)$, where k_B is Boltzmann's constant and $e_i = \hbar \nu_i$ is the energy related to normal mode ν_i. H_2 is considered as an ideal gas, the enthalpy consists of the ZPE term and the vibrational contributions [14] according to the equation; $F^{vib}(T)_{H_2} = \frac{1}{2} \cdot e_0 + \frac{7}{2} k_B T + \frac{e_0}{e^{-\beta \cdot e_0} - 1}$ while the entropy is calculated using the experimental data by Hemmes *et al.* [15].

Plane-wave cutoff convergence tests for $Na_2B_{12}H_{12}$ and $Li_2B_{12}H_{12}$

The convergence with respect to cutoff energy indicate that the total energy changes less that 0.1% between 500 eV and 800 eV, see Fig. S1. The change of the cell volume is larger but it is less than 2% for cutoff range between 500 eV and 800 eV, Fig. S2. In Table ST1 (ESI†) changes of the lattice parameters for $Li_2B_{12}H_{12}$ and $Na_2B_{12}H_{12}$ between 500 eV and 800 eV plane wave basis set cutoff. For the calculations of properties use the kinetic energy cutoff of 500 eV as this is closer to calculations setting used for molecular dynamics calculations of the high temperature phases and the errors due to this cutoff energy are small.

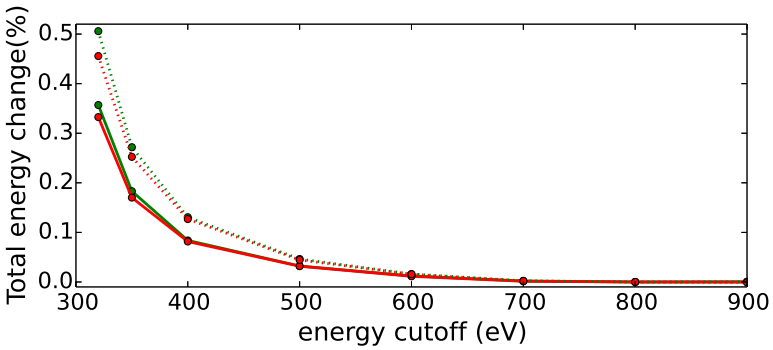

Figure S1 The change of the total energy with respect to the plane-wave energy cutoff. The total energy for cutoff=800eV is taken as a reference. $Li_2B_{12}H_{12}$ and $Na_2B_{12}H_{12}$ results are denoted with red and green respectively. The dashed lines denote the results using the vdW-DF and the solid ones are for the PBE functional. The energy cutoff=500eV used throughout the calculations of $Li_2B_{12}H_{12}$ and $Na_2B_{12}H_{12}$. Lines are guide to the eye.

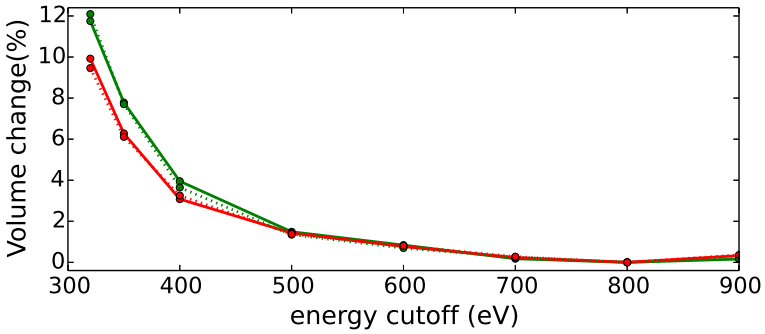

Figure S2 The change of the volume ($\frac{V_{500eV}-V_{800eV}}{V_{800eV}} * 100$) with respect to the plane-wave energy cutoff. $Li_2B_{12}H_{12}$ and $Na_2B_{12}H_{12}$ results are denoted with red and green lines respectively. The dashed lines denote the results for the vdW-DF functional, and the solid lines are the PBE functional. The cutoff=500eV used throughout the calculations of $Li_2B_{12}H_{12}$ and $Na_2B_{12}H_{12}$. Lines are guide to the eye.

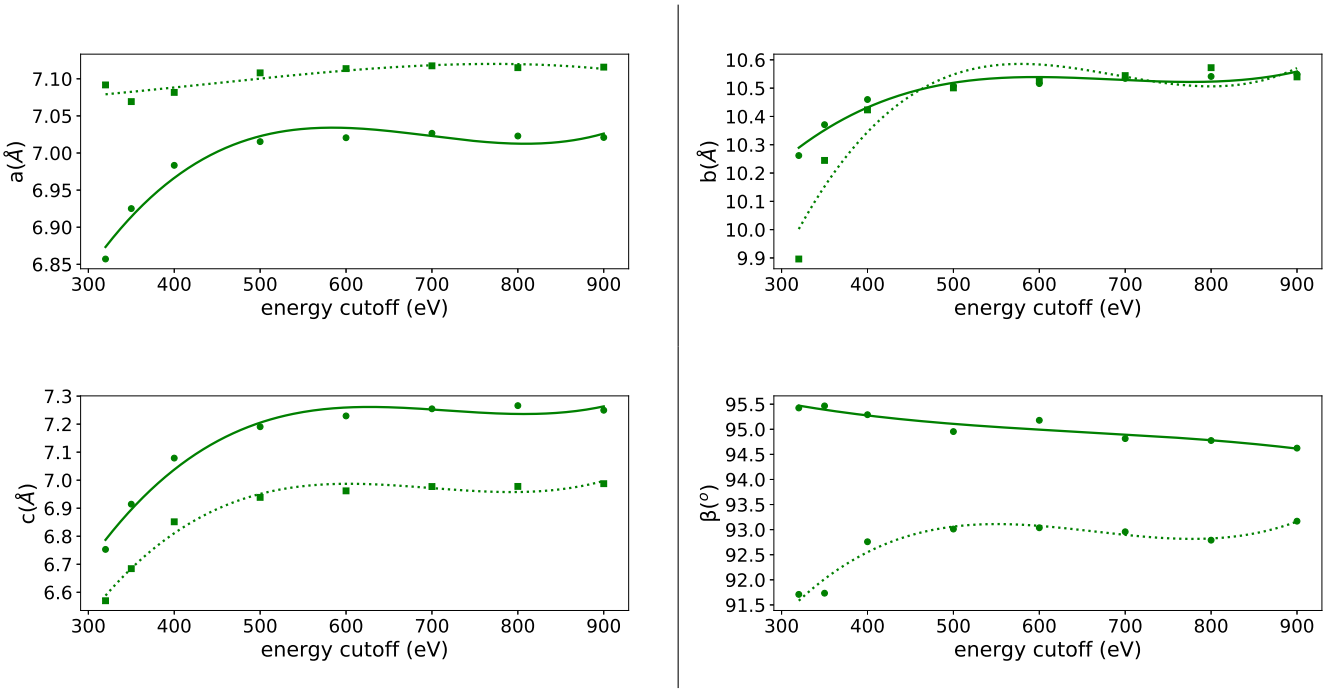

Figure S3 Convergence plot of the $Na_2B_{12}H_{12}$ lattice parameters in respect to the plane-wave energy cutoff. The results of the vdW-DF and the PBE functional are denoted with dashed lines/squares and solid lines/circles respectively. Lines are guide to the eye.

	$Na_2B_{12}H_{12}$		$Li_2B_{12}H_{12}$	
parameter	**PBE**	**vdW-DF**	**PBE**	**vdW-DF**
volume	1.48	1.35	1.43	1.37
B_{12} volume	0.07	0.09	0.07	0.09
a	0.11	0.10	0.48	0.46
b	0.32	0.67	0.48	0.46
c	1.04	0.56	0.48	0.46
β	0.19	0.24	0.00	0.00
B-H distance	0.04	0.06	0.06	0.06
B-B distance	0.03	0.04	0.07	0.05

Table ST1 Percentage changes for the lattice and structural parameters of $Na_2B_{12}H_{12}$ and $Li_2B_{12}H_{12}$, with vdW-DF and PBE functionals. Comparing two values of plane-wave cutoff, 500 eV and 800 eV. The small changes in the B_{12} volume, and the B-H and B-B distances, ensure that the distortion of the B_{12} cage as well as the phonon population are not strongly dependent on the plane-wave cutoff energy in the range 500 eV and 800 eV.

compound	symmetry	method	a(Å)	b(Å)	c(Å)	$\beta(^o)$	V/Z (Å^3)	B_{12} volume(Å^3)	$B_{12}H_{12}$ charge (e)
$Li_2B_{12}H_{12}$									
	P$a\bar{3}$	experiment[†]	9.577	9.577	9.577	90.000	219.61	12.689	
	P$a\bar{3}$	PBE[16]	9.577	9.577	9.577	90.000	219.61		
	P$a\bar{3}$	PW91[17]	9.600	9.600	9.600	90.000	221,18		
	P$a\bar{3}$	PBE[18]	9.623	9.623	9.623	90.000	222.78		
	P$a\bar{3}$	PBE[19]	9.634	9.634	9.634	90.000	223.54		
	P$a\bar{3}$	PBE	9.598	9.598	9.598	90.000	221.01	12.243	-1.90
	P$a\bar{3}$	LDA	9.192	9.192	9.192	90.000	194.14	11.825	-1.87
	P$a\bar{3}$	PBE-D2	9.038	9.038	9.038	90.000	184.57	12.191	-1.88
	P$a\bar{3}$	PBE-D3(BJ)	9.288	9.288	9.288	90.000	200.32	12.124	-1.92
	P$a\bar{3}$	vdW-DF	9.644	9.644	9.644	90.000	224.22	12.483	-1.90
	P$a\bar{3}$	PBE-D2[*]	9.644	9.644	9.644	90.000	224.22	12.465	-1.90
	P$a\bar{3}$	PBE0	9.528	9.528	9.528	90.000	216.24	12.095	-1.80
	P$a\bar{3}$	HSE06	9.563	9.563	9.563	90.000	218.60	12.097	-1.90
$Na_2B_{12}H_{12}$									
	P$2_1/n$	experiment[†]	7.031	10.654	7.009	94.676	261.64	12.459	
	P$2_1/n$	experiment[‡]	6.975	10.537	6.956	95.959	254.22	12.240	
	P$2_1/n$	experiment[§]	7.050	10.732	7.071	93.570	268.65	12.151	
	P$2_1/n$	PBE[20]	6.964	10.657	7.242	93.988			
	P$2_1/n$	PBE[16]	7.031	10.654	7.009	94.676			
	P$2_1/c$	PBE[19]	7.056	10.601	7.296	95.146			
	P$2_1/c$	PBE[21,22]	7.027	10.591	6.857	95.343			
	P$2_1/n$	PBE	7.015	10.507	7.191	94.954	264.04	12.272	-1.84
	P$2_1/n$	LDA	6.743	10.128	6.731	96.865	228.18	11.843	-1.83
	P$2_1/n$	PBE-D2	6.673	10.166	6.581	97.706	221.20	12.243	-1.82
	P$2_1/n$	PBE-D3(BJ)	6.850	10.284	6.765	95.754	237.11	12.168	-1.86
	P$2_1/n$	vdW-DF	7.108	10.501	6.939	93.012	258.60	12.513	-1.85
	P$2_1/n$	PBE-D2[*]	7.108	10.501	6.939	93.012	258.60	12.438	-1.89
	P$2_1/n$	PBE0	6.969	10.436	7.131	95.266	258.21	12.124	-1.72
	P$2_1/n$	HSE06	6.977	10.445	7.160	95.410	259.73	12.126	-1.72

Table ST2 Structural details and charge distribution analysis for $Li_2B_{12}H_{12}$ and $Na_2B_{12}H_{12}$ for the low temperature phases, P$a\bar{3}$ and P$2_1/c$ respectively. For $Li_2B_{12}H_{12}$ other symmetries, such as P$2_1/n$[23], C2/m[18,24] and for $Na_2B_{12}H_{12}$ other symmetries, such as I$m\bar{3}m$[19] and P$a\bar{3}$[20] have been investigated but are not observed in low temperature experiments. For lattice parameters $\alpha = \gamma = 90^o$. B_{12} volume stands for the volume of the boron cage in the $B_{12}H_{12}{}^{2-}$ anion. The charge of anions was calculated with Bader charge analysis (as implemented by Henkelman *et al.*[5]). For these calculations the fine charge density support grid was used (eight times denser than the standard grid). P$2_1/n$ is the more orthogonal, non-standard representation of the P$2_1/c$ space group and notations are often interchanged.

[†]: experimental results in ambient temperature for $Li_2B_{12}H_{12}$[25] and $Na_2B_{12}H_{12}$[26]

[‡]: $Na_2B_{12}H_{12}$ experimental results at 7K[27]

[§]: $Na_2B_{12}H_{12}$ experimental results at 298K[27]

Besides obvious parameters like exchange correlation functional, plane wave cutoff, type of pseudopotentials or density of k-point sampling, a variety of factors related to practical implementation of DFT affect the calculated ground state lattice parameters. To name a few they are: representation/density of the charge grid, non-spherical contribution to charge density gradients, expansion of the kinetic energy density and others. Therefore, differences of the order of 0.1% might be expected for such complex systems like M-$B_{12}H_{12}$ compounds considered in this work. For the $Li_2B_{12}H_{12}$ the previous results summarized in Table ST3. The referenced reports relay on

Reference	a(Å)	Difference(%)
Present study	**9.598**	**-**
Varley *et al.* [19]	9.634	0.4%
Kweon *et al.* [28]	9.630	0.3%
Li *et al.* [18]	9.623	0.3%
Verdal *et al.* [16a]	9.577	0.2%

Table ST3 Comparison of lattice parameters from previous calculations of $Li_2B_{12}H_{12}$ with the present study results of PBE.

[a] experimental lattice from Her *et al.* [25]

different methodology/implementations:

Varley *et al.* [19]; *ab initio* molecular dynamics simulations (AIMD) through the Quantum Espresso code in the P$m\bar{3}n$ symmetry structure with the PBE functional and ultrasoft Rappe-Rabe-Kaxiras-Joannopoulos (rrkjus) pseudopotentials,

Kweon *et al.* [28]; AIMD, the Quantum Espresso code in the P$m\bar{3}n$ symmetry with the PBE functional and ultrasoft rrkjus pseudopotentials,

Li *et al.* [18]; the PBE exchange correlation functional with VASP code. Using the same k-point grid and plane-wave cutoff as the authors of this paper we obtain a=9.635Å, which differs by 0.1% with the value of Li *et al.* [18],

Verdal *et al.* [16]; the experimental lattice parameters from Her *et al.* [25] with the PWscf software package.

For the $Na_2B_{12}H_{12}$ structure, results from previous calculations are summarized in Table ST4.

Reference	a(Å)	Diff(%)	b(Å)	Diff(%)	c(Å)	Diff(%)	$\beta(^o)$	Diff(%)
Present study	**7.015**	**-**	**10.507**	**-**	**7.191**	**-**	**94.954**	**-**
Caputo *et al.* [20]	6.9639	0.7	10.6569	1.4	7.2421	0.7	93.9883	1.0
Verdal *et al.* [16]	7.031	0.2	10.654	1.4	7.009	2.6	94.676	0.3
Lu *et al.* [21]	7.027	0.2	10.591	0.8	6.857	4.9	95.343	0.4
Varley *et al.* [19]	7.056	0.6	10.601	0.9	7.296	1.4	95.146	0.2

Table ST4 Comparison of lattice parameters from previous calculations of $Na_2B_{12}H_{12}$ with the present study results of PBE.

Caputo *et al.* [20]; PBE in the $P2_1/n$, CASTEP, as implemented in Materials Studio 5.0,

Verdal *et al.* [16]; PWscf package, the lattice parameters used for $Na_2B_{12}H_{12}$ are the experimental values of Her *et al.* [26],

Lu *et al.* [21] refers to the structure presented in the Materials Project Database with ID mp-978278 [22]. Different pseudopotentials, k-point grids,

Varley *et al.* [19]; AIMD in the Quantum Espresso code different cutoff and k-point sampling.

The previously proposed C2/m structure for $MgB_{12}H_{12}$ by Ozoliņš *et al.* [24], calculated with VASP software, differs by 1.4%, 4.3%, 0.1% and 0.9% for a, b, c and β lattice parameters respectively

and there is a 5.3% difference in the cell volume (compared to the present C2/m structure, as calculated with the PBE functional). Using the plane-wave cutoff and k-point grid as in the paper by Ozoliņš *et al.* [24] the differences with our results is 0.8%, 2.0%, 0.1% and 2.5% for the a, b, c and β lattice parameters, while the volume of the unit cell has a 0.3% difference.

A quasi-harmonic approximation could also affect the equilibrium lattice parameters, when the phonon population is taken into account. However, the interplay between quasi-harmonic properties and configurational entropy (cation distribution within tetrahedral voids) is far beyond the scope of the present manuscript and require a separate study.

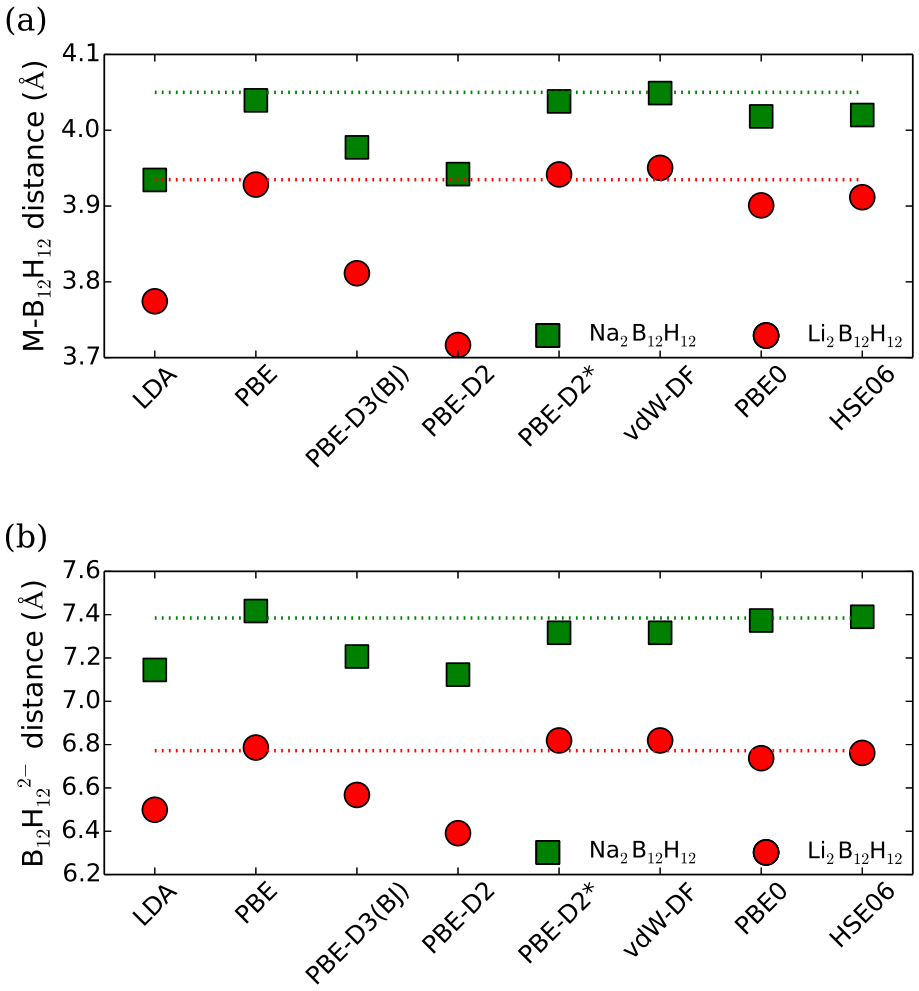

Figure S4 (a) Distance between metal and the center of the $B_{12}H_{12}^{2-}$ anion and (b) distance between the centers of $B_{12}H_{12}^{2-}$ anions for $Li_2B_{12}H_{12}$ and $Na_2B_{12}H_{12}$. The dashed green and red lines refer to the experimental data of $Na_2B_{12}H_{12}$ [27](7K) and $Li_2B_{12}H_{12}$ [25] in ambient temperature.

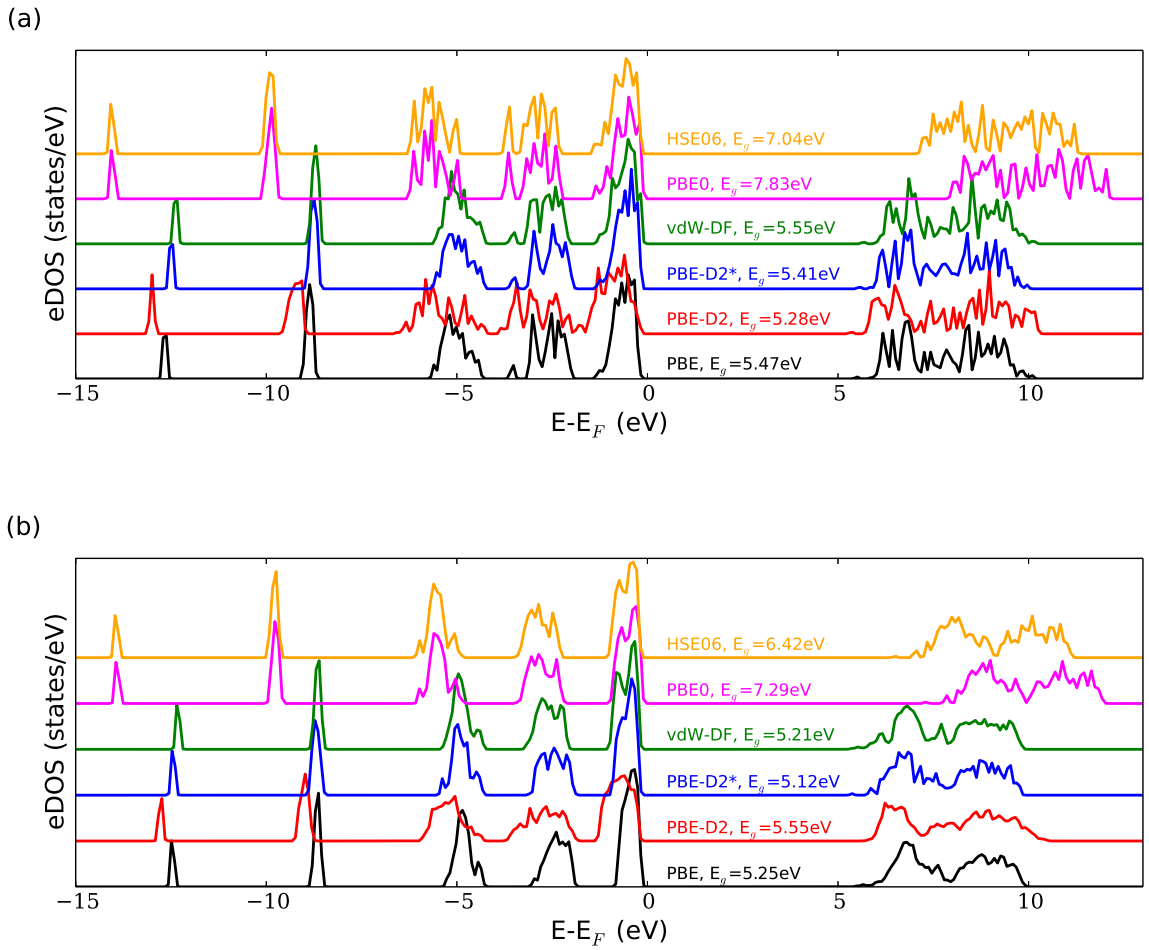

Figure S5 Electronic density of states(eDOS) for (a) $Li_2B_{12}H_{12}$ and (b) $Na_2B_{12}H_{12}$ with PBE (black), PBE-D2(red), PBE-D2*(blue) , vdW-DF(green), PBE0(magenta) and HSE06(orange). The band gaps (E_g) for each method and compound are indicated in the legend of each graph. Hybrid functionals, PBE0 and HSE06 give bigger band gaps as expected. Otherwise, a 5% and 8% dispersion between the methods can be observed for $Li_2B_{12}H_{12}$ and $Na_2B_{12}H_{12}$ respectively. The smaller volume for PBE-D2 results in the shift of the eDOS.

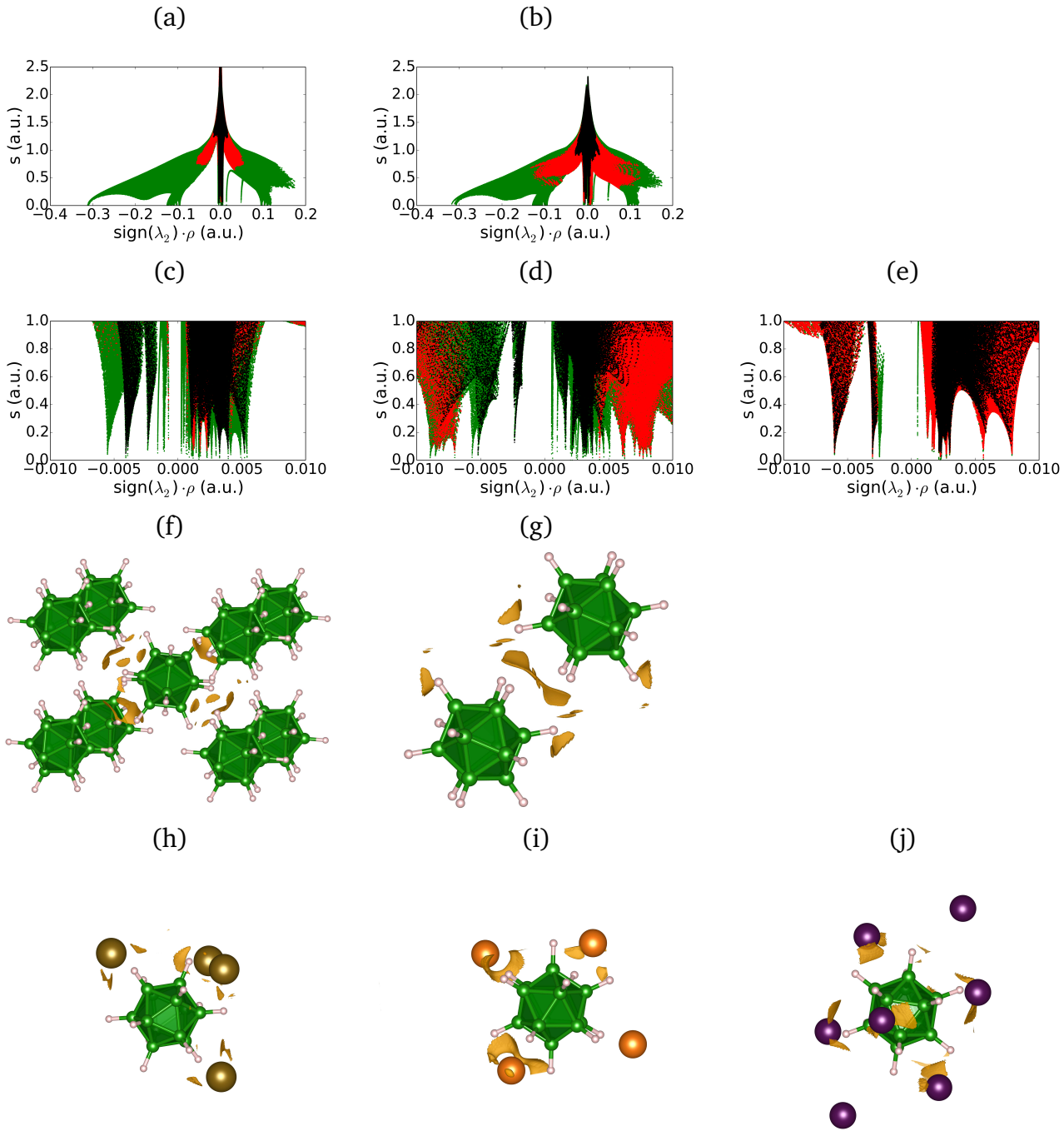

Figure S6 In graphs (a) and (b) we show the reduced density gradient(RDG) index(green) for $Na_2B_{12}H_{12}$ and $MgB_{12}H_{12}$ ($C2/c$ symmetry) structures. The reduced density gradient corresponding to the interaction between the cations and one of the anions of the unit cell is denoted with red and the interaction between two neighbouring anions is denoted with black. Graphs (c) (d) and (e) focus on the region representing weak interactions(-0.01<ρ<0.01 a.u.) for $Na_2B_{12}H_{12}$, $MgB_{12}H_{12}$ and $Li_2B_{12}H_{12}$ respectively. Graphs (f) and (g) visualize the isosurface(yellow) that corresponds to the weak interaction between two neighbouring anions of the unit cell(green polyhedra). For better visualization the additional periodic atoms are also shown. Graphs (h), (i) and (j) show the isosurface(yellow) that corresponds to the weak interaction between an anion and the cations of the unit cell for $Na_2B_{12}H_{12}$, $MgB_{12}H_{12}$ and $Li_2B_{12}H_{12}$. The visualization of all the isosurfaces corresponds to s=0.5 a.u. and -0.01<ρ<0.01 a.u., while the atoms in the unit cell are shifted such as that the referred anions are located in its center for a more clear visualization.

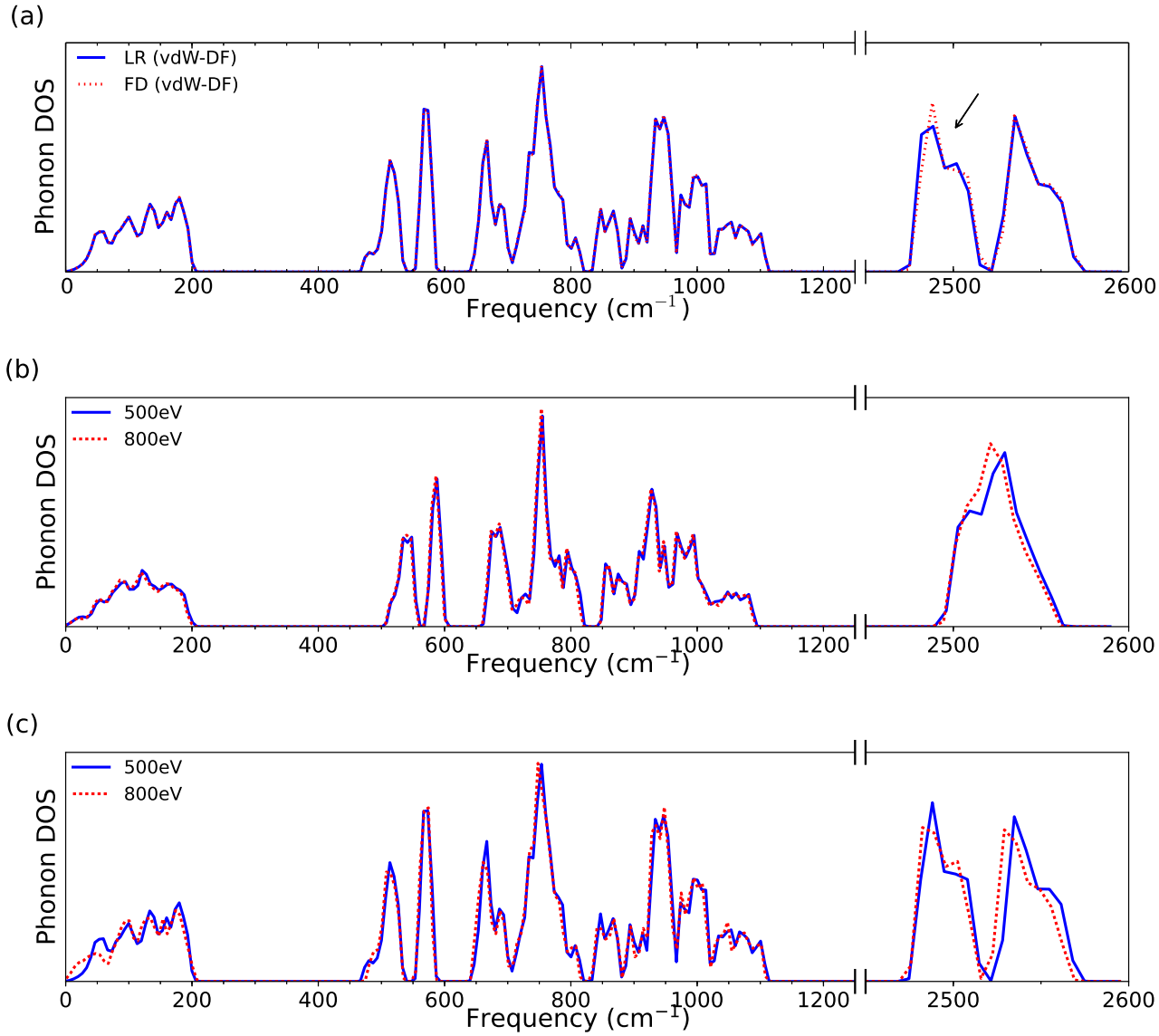

Figure S7 Phonon density of states of $Na_2B_{12}H_{12}$ with the vdW-DF method comparing the two different methods: finite differences (FD) and linear response (LR) (a). The black arrow indicates the area where the visible differences in the spectra are present. (b) Phonon density of states of $Na_2B_{12}H_{12}$ with PBE functional and two energy cutoffs. (c) Phonon density of states of $Na_2B_{12}H_{12}$ with vdW-DF functional and two energy cutoffs. Only the minor changes in the lattice and B-H stretching mode regions can be observed.

Atom	site	positions
Mg	2c	(0.000, 0.000, 0.500)
B	8j	(-0.087, 0.192, 0.88); (0.053, 0.117, 0.855)
	4i	(0.893, 0.000, 0.721); (0.826, 0.000, 0.900)
H	8j	(0.855, 0.324, 0.797); (0.088, 0.197, 0.741)
	4i	(0.823, 0.000, 0.518); (0.707, 0.000, 0.834)

Table ST5 $MgB_{12}H_{12}$ structure with C2/m (# 12, Z = 2) symmetry, $a = 11.427$ Å, $b = 7.684$ Å, $c = 6.946$ Å, $\beta = 120.898^{\circ}$.

Atom	site	positions
Mg	4e	(0.000, 0.877, 0.250)
B	8f	(0.842, 0.135, 0.410); (0.793, 0.255, 0.657)
		(0.812, 0.440, 0.560); (0.093, 0.254, -0.043)
		(0.842, 0.365, 0.405); (0.313, 0.434, 0.064)
H	8f	(-0.091, 0.058, 0.344); (0.825, 0.257, 0.769)
		(0.354, 0.071, 0.602); (-0.019, 0.254, -0.074)
		(-0.094, 0.440, 0.339); (0.860, 0.061, 0.111)

Table ST6 $MgB_{12}H_{12}$ structure with $C2/c$ (# 15, Z = 4) symmetry, $a = 10.621$ Å, $b = 7.835$ Å, $c = 10.626$ Å, $\beta = 95.343^{\circ}$.

Atom	site	positions
Mg	2f	(0.500, 0.500, 0.250)
B	8k	(0.128, 0.469, 0.650); (-0.049, 0.289, 0.594)
	4j	(0.683, 0.176, 0.000); (0.421, 0.235, 0.000)
H	8k	(0.211, 0.449, 0.762); (-0.089, 0.148, 0.660)
	4j	(0.809, 0.300, 0.000); (0.360, 0.402, 0.000)

Table ST7 $MgB_{12}H_{12}$ structure with $P4_2/m$ (# 84, Z = 2) symmetry, $a = 6.781$ Å, $c = 9.519$ Å.

Atom	site	positions
Mg	4d	(0.424, 0.250, 0.250)
B	8e	(0.700, 0.312, 0.815);(0.570, 0.392, 0.749)
		(0.569, 0.313, -0.034);(0.437, 0.314, 0.814)
		(0.490, 0.311, 0.577);(0.651, 0.314, 0.573)
H	8e	(0.794, 0.359, 0.856);(0.568, 0.357, 0.121)
		(0.207, 0.142, -0.050);(-0.068, 0.140, -0.043)
		(0.430, 0.511, 0.251);(0.846, 0.360, 0.146)

Table ST8 $MgB_{12}H_{12}$ structure with Pnna (# 52, Z = 4) symmetry, $a = 11.006$ Å, $b = 12.144$ Å, $c = 7.037$ Å.

Atom	site	positions
Mg	2a	(0.725, 0.608, 0.579)
B	2a	(0.761, 0.873, 0.485);(-0.056, 0.846, 0.316)
		(0.536, -0.081, 0.360);(0.697, 0.790, 0.266)
		(0.578, -0.082, 0.112);(0.832, 0.874, 0.088)
		(0.575, 0.080, 0.241);(-0.022, 0.011, 0.202)
		(0.755, 0.055, 0.073);(0.818, 0.139, 0.296)
		(-0.066, 0.007, 0.445);(0.684, 0.053, 0.474)
H	2a	(0.765, 0.814, 0.636);(0.075, 0.766, 0.342)
		(0.379, 0.889, 0.422);(0.657, 0.665, 0.259)
		(0.451, 0.889, -0.002);(0.888, 0.812, -0.044)
		(0.446, 0.166, 0.211);(0.137, 0.044, 0.147)
		(0.753, 0.121, -0.069);(0.857, 0.261, 0.305)
		(0.057, 0.033, 0.571);(0.630, 0.113, 0.609)

Table ST9 $MgB_{12}H_{12}$ structure with $P2_1$ (# 4, Z = 2) symmetry, $a = 6.805$ Å, $b = 9.496$ Å, $c = 7.121$ Å, $\beta = 92.896^{\circ}$.

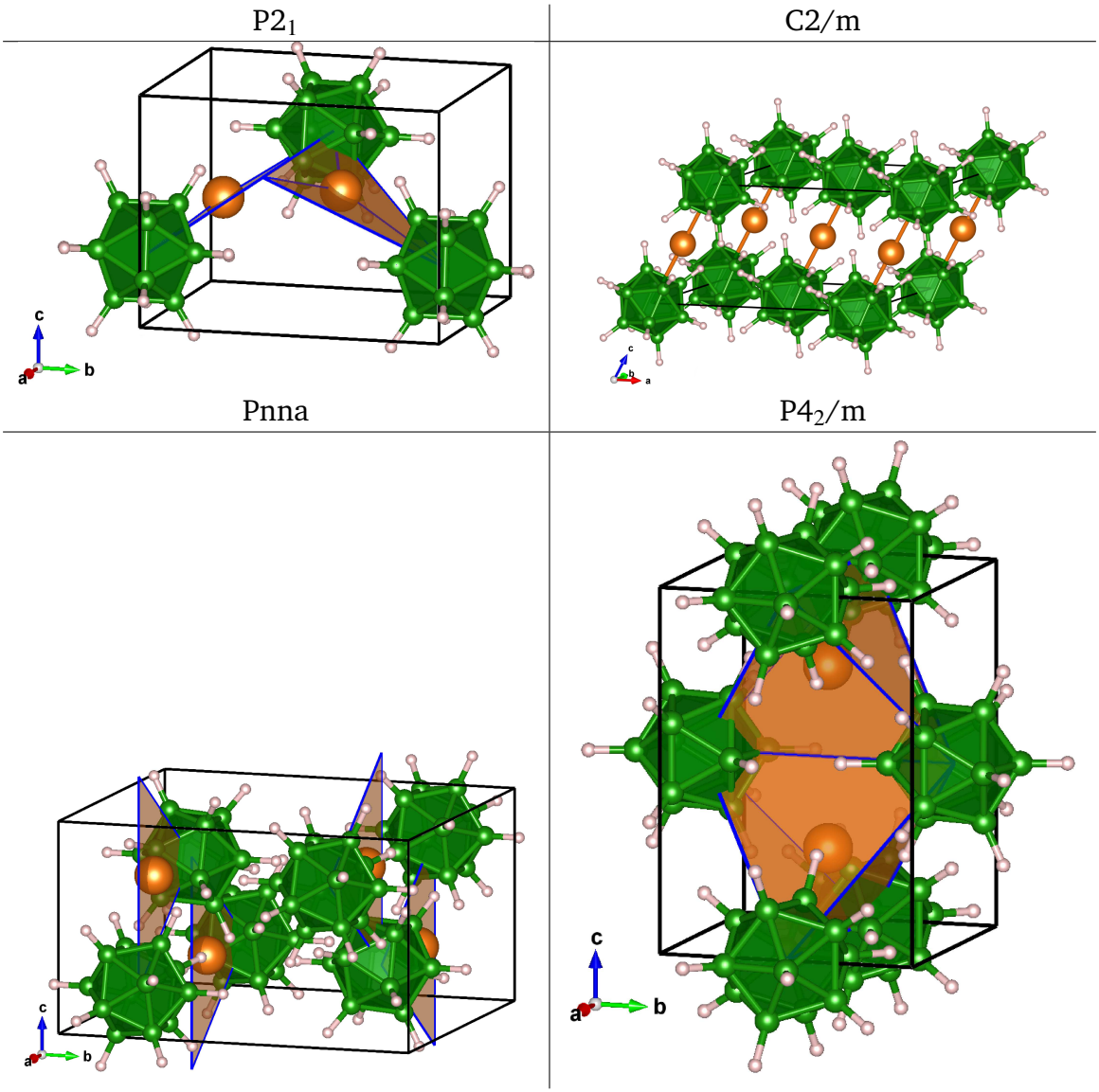

Figure S8 $MgB_{12}H_{12}$ structures. Magnesium, boron and hydrogen atoms are denoted with orange, green and light pink color, while the orange planes indicate the coordination of Mg in each structure. Details on each structure are presented in tables ST5, ST7, ST8 and ST9 for C2/m, $P4_2/m$, Pnna and $P2_1$ symmetry respectively. As indicated in the figures, we observe linear coordination of Mg in the C2/m symmetry, tetragonal coordination in $P4_2/m$ and trigonal planar in Pnna(in the same plane) and $P2_1$(in different planes). For better visualization, neighbouring atoms, outside of the unit cell are also displayed.

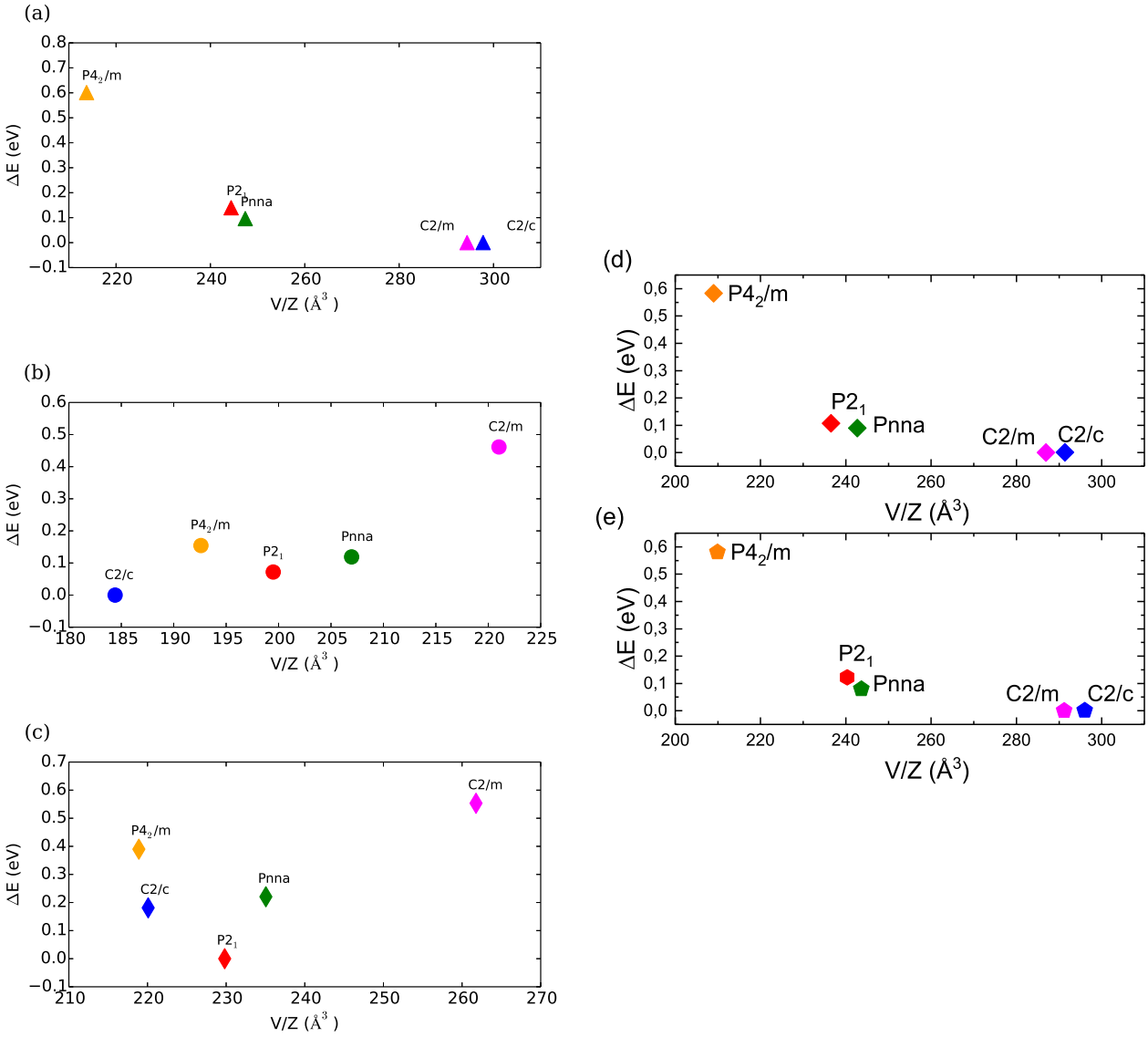

Figure S9 The ground state energy per formula unit for $MgB_{12}H_{12}$ shown as a difference with respect to the lowest energy for given exchange correlation functional: PBE (a), PBE-D2 (b), PBE-D2* (c), PBE0 (d) and HSE06(e). The horizontal axis refers to volume per formula unit.

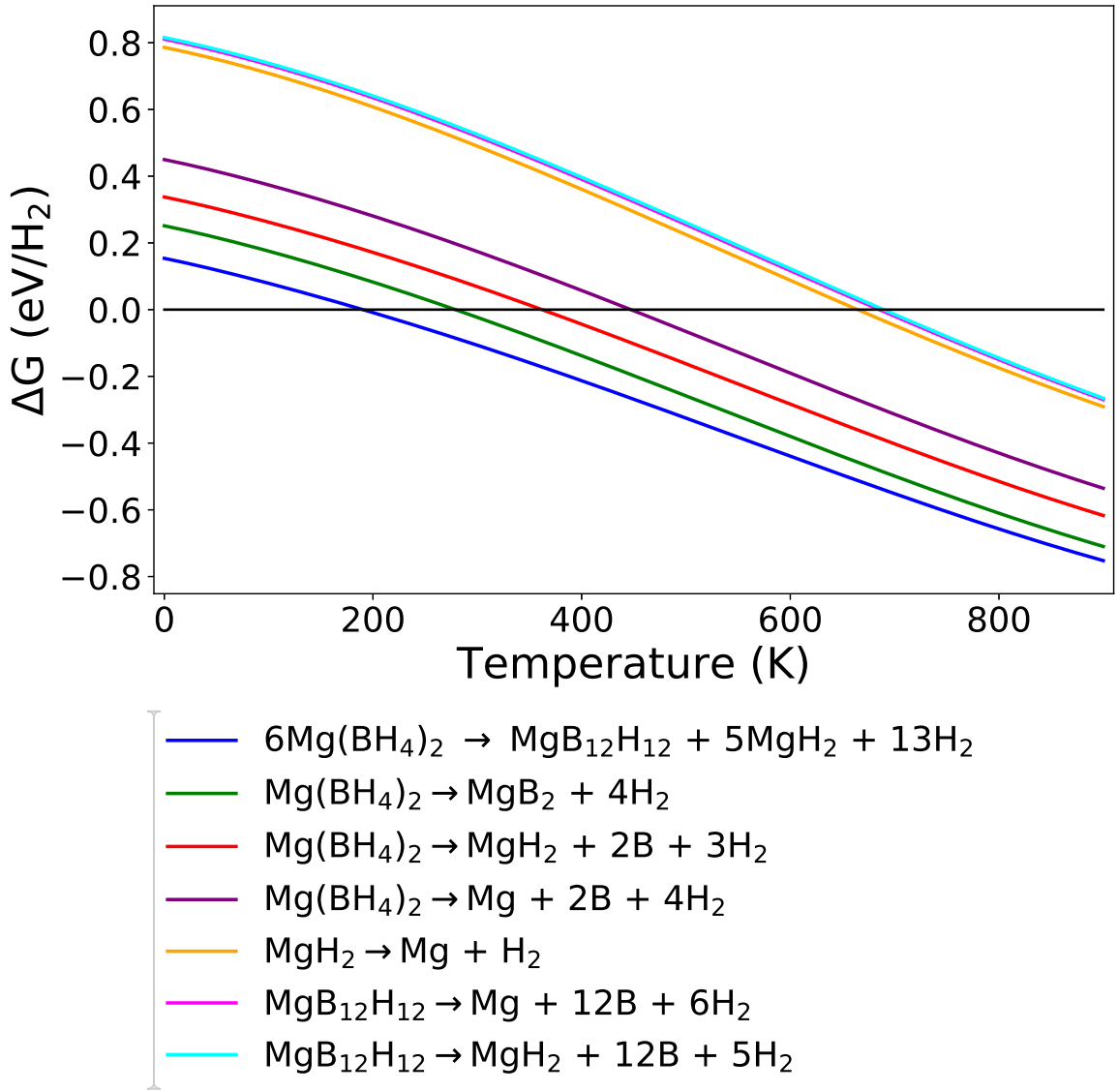

Figure S10 The Gibbs free energy (eV/H_2) for various decomposition pathways of $Mg(BH_4)_2$ and $MgB_{12}H_{12}$ with the vdW-DF method. The reference $Mg(BH_4)_2$ structure is $I4_1/amd$ (# 141) phase; according to Bil *et al.*[29] it has a ground state energy ΔE=0.047 eV/BH_4 larger than the experimental α phase ($P6_122$ (# 178) with 30 formula units/unit cell)

Elastic Properties of the $MgB_{12}H_{12}$ structures

The stress(σ)-strain(e) relation, according to Hooke's law, can be expressed as $\sigma_{ij} = C_{ijkl} \cdot e_{kl}$, where C_{ijkl} is a fourth-order elasticity tensor with 81 independent elastic constants[30]. By following the Voigt notation, (11$\mapsto$1, 22$\mapsto$2, 33$\mapsto$3, 23$\mapsto$4, 13$\mapsto$5 and 12$\mapsto$6) the terms are compacted to $\sigma_i = C_{ij} \cdot e_j$. Following the symmetries the tensor is reduced to 21 elastic moduli, with its extended form shown in equation 6.

$$\begin{bmatrix} \sigma_x \\ \sigma_y \\ \sigma_z \\ \tau_{yz} \\ \tau_{zx} \\ \tau_{xy} \end{bmatrix} = \begin{bmatrix} C_{11} & C_{12} & C_{13} & C_{14} & C_{15} & C_{16} \\ C_{21} & C_{22} & C_{23} & C_{24} & C_{25} & C_{26} \\ C_{31} & C_{32} & C_{33} & C_{34} & C_{35} & C_{36} \\ C_{41} & C_{42} & C_{43} & C_{44} & C_{45} & C_{46} \\ C_{51} & C_{52} & C_{53} & C_{54} & C_{55} & C_{56} \\ C_{61} & C_{62} & C_{63} & C_{64} & C_{65} & C_{66} \end{bmatrix} \cdot \begin{bmatrix} e_x \\ e_y \\ e_z \\ 2e_{yz} \\ 2e_{zx} \\ 2e_{xy} \end{bmatrix} \tag{6}$$

This elastic tensor is calculated for each structure using finite differences as implemented in VASP for the calculation of the elastic moduli and additionally by increasing the energy cutoff (700eV) and doubling the k-points in each direction (compared to the energy calculations) and also an additional support grid for the evaluation of the augmentation charges implemented in VASP was enabled. Each structure is relaxed anew in these parameters.

The Voigt-Reuss-Hill average is calculated as $G_{VRH} = (G_V + G_R)/2$ for the shear modulus and as $K_{VRH} = (K_V + K_R)/2$ for the bulk modulus. As defined[31], the Voigt value for the shear modulus is:

$$G_V = ((C_{11} + C_{22} + C_{33}) - (C_{12} + C_{23} + C_{31}) + (3 \cdot (C_{44} + C_{55} + C_{66})))/15. \tag{7}$$

the Reuss value is :

$$G_R = 15/(4 \cdot (s_{11} + s_{22} + s_{33}) - 4 \cdot (s_{12} + s_{23} + s_{31}) + (3 \cdot (s_{44} + s_{55} + s_{66}))), \tag{8}$$

respectively the values for the bulk moduli are:

$$K_V = ((C_{11} + C_{22} + C_{33}) + 2 \cdot (C_{12} + C_{23} + C_{31}))/9. \tag{9}$$

and

$$K_R = 1./((s_{11} + s_{22} + s_{33}) + 2 \cdot (s_{12} + s_{23} + s_{31})) \tag{10}$$

where $s_{ij} = C_{ij}^{-1}$

Additionally, the Poisson's ratio μ is calculated according to the equation:

$$\mu = \frac{3 \cdot K_{VRH} - 2 \cdot G_{VRH}}{6 \cdot K_{VRH} + 2 \cdot G_{VRH}} \tag{11}$$

In table ST10 the values for all the quantities mentioned above are presented for the five structures of $MgB_{12}H_{12}$.

Structure	**C2/c**	**C2/m**	**$P2_1$**	**$P4_2/m$**	**Pnna**
K_V (GPa)	28.45	18.32	15.67	26.15	24.01
K_R (GPa)	19.36	8.68	13.31	24.63	15.35
K_{VHR} (GPa)	**23.91**	**13.50**	**14.49**	**25.39**	**19.68**
G_v (GPa)	14.84	10.06	11.76	15.89	13.09
G_R (GPa)	10.75	2.32	8.44	13.34	8.47
G_{VHR} (GPa)	**12.79**	**6.19**	**10.10**	**14.62**	**10.78**
Poisson's ratio μ	0.27	0.30	0.22	0.26	0.27

Table ST10 Elastic properties of the $MgB_{12}H_{12}$ structures calculated with vdW-DF. The Voigt-Reuss-Hill average for the bulk modulus (K_{VRH}) and the shear modulus (G_{VRH}) as well as the Poisson's ratio (μ) are presented. The individual values for the Voigt and the Reuss bulk and shear modulus provide an upper and lower limit for each modulus.

Bibliography

[1] P. E. Blöchl, *Phys. Rev. B*, 1994, **50**, 17953–17979.

[2] G. Kresse and D. Joubert, *Phys. Rev. B*, 1999, **59**, 1758–1775.

[3] J. P. Perdew and A. Zunger, *Phys. Rev. B*, 1981, **23**, 5048–5079.

[4] J. P. Perdew, K. Burke and M. Ernzerhof, *Phys. Rev. Lett.*, 1996, **77**, 3865–3868.

[5] G. Henkelman, A. Arnaldsson and H. Jónsson, *Comput. Mater. Sci.*, 2006, **36**, 354 – 360.

[6] E. R. Johnson, S. Keinan, P. Mori-Sánchez, J. Contreras-García, A. J. Cohen and W. Yang, *J. Am. Chem. Soc.*, 2010, **132**, 6498–6506.

[7] A. Otero-de-la-Roza, E. R. Johnson and J. Contreras-Garcia, *Phys. Chem. Chem. Phys.*, 2012, **14**, 12165–12172.

[8] A. Otero-de-la-Roza, M. Blanco, A. M. Pendás and V. L. na, *Comput. Phys. Commun.*, 2009, **180**, 157 – 166.

[9] A. Otero-de-la-Roza, E. R. Johnson and V. L. na, *Comput. Phys. Commun.*, 2014, **185**, 1007 – 1018.

[10] A. Togo and I. Tanaka, *Scr. Mater.*, 2015, **108**, 1–5.

[11] M. Gajdoš, K. Hummer, G. Kresse, J. Furthmüller and F. Bechstedt, *Phys. Rev. B*, 2006, **73**, 045112.

[12] M. J. van Setten, G. A. de Wijs, M. Fichtner and G. Brocks, *Chem. Mater.*, 2008, **20**, 4952–4956.

[13] D. Harrison and T. Thonhauser, *Phys. Rev. B*, 2014, **90**, 125152.

[14] L. G. Hector, J. F. Herbst, W. Wolf, P. Saxe and G. Kresse, *Phys. Rev. B*, 2007, **76**, 014121.

[15] H. Hemmes, A. Driessen and R. Griessen, *J. Phys. C: Solid State Phys.*, 1986, **19**, 3571.

[16] N. Verdal, W. Zhou, V. Stavila, J.-H. Her, M. Yousufuddin, T. Yildirim and T. J. Udovic, *J. Alloys Compd.*, 2011, **509**, S694 – S697.

[17] Y. Wang, Y. Zhang and C. Wolverton, *Phys. Rev. B*, 2013, **88**, 024119.

[18] S. Li, X. Ju and C. Wan, *J. Alloys Compd.*, 2014, **593**, 169 – 175.

[19] J. B. Varley, K. Kweon, P. Mehta, P. Shea, T. W. Heo, T. J. Udovic, V. Stavila and B. C. Wood, *ACS Energy Letters*, 2017, **2**, 250–255.

[20] R. Caputo, S. Garroni, D. Olid, F. Teixidor, S. Surinach and M. D. Baro, *Phys. Chem. Chem. Phys.*, 2010, **12**, 15093–15100.

[21] Z. Lu and F. Ciucci, *Chem. Mater.*, 2017, **29**, 9308–9319.

[22] K. Persson, *Materials Data on Na(BH)6 (SG:14) by Materials Project*, 2016.

[23] N. Ohba, K. Miwa, M. Aoki, T. Noritake, S.-i. Towata, Y. Nakamori, S.-i. Orimo and A. Züttel, *Phys. Rev. B*, 2006, **74**, 075110.

[24] V. Ozoliņš, E. H. Majzoub and C. Wolverton, *J. Am. Chem. Soc.*, 2009, **131**, 230–237.

[25] J.-H. Her, M. Yousufuddin, W. Zhou, S. S. Jalisatgi, J. G. Kulleck, J. A. Zan, S.-J. Hwang, R. C. Bowman and T. J. Udovic, *Inorg. Chem.*, 2008, **47**, 9757–9759.

[26] J.-H. Her, W. Zhou, V. Stavila, C. M. Brown and T. J. Udovic, *J. Phys. Chem. C*, 2009, **113**, 11187–11189.

[27] N. Verdal, J.-H. Her, V. Stavila, A. V. Soloninin, O. A. Babanova, A. V. Skripov, T. J. Udovic and J. J. Rush, *J. Solid State Chem.*, 2014, **212**, 81 – 91.

[28] K. E. Kweon, J. B. Varley, P. Shea, N. Adelstein, P. Mehta, T. W. Heo, T. J. Udovic, V. Stavila and B. C. Wood, *Chem. Mater.*, 0, **0**, null.

[29] A. Bil, B. Kolb, R. Atkinson, D. G. Pettifor, T. Thonhauser and A. N. Kolmogorov, *Phys. Rev. B*, 2011, **83**, 224103.

[30] M. H. Sadd, *Elasticity: theory, applications, and numerics*, Academic Press, 2009.

[31] R. Hill, *Proc. Phys. Soc. London, Sect. A*, 1952, **65**, 349.